TECHNICAL MEMORANDUMS

NATIONAL ADVISORY COMMITTEE FOR AERONAUTICS

No. 798

FLOW PHENOMENA ON PLATES AND AIRFOILS OF SHORT SPAN

By H. Winter

Verein Deutscher Ingenieure
Special Issue (Aviation), 1936

Washington
July 1936

NATIONAL ADVISORY COMMITTEE FOR AERONAUTICS

TECHNICAL MEMORANDUM NO. 798

FLOW PHENOMENA ON PLATES AND AIRFOILS OF SHORT SPAN

By H. Winter

SUMMARY

Investigations on the flow phenomena at plates and cambered models were carried out with the aid of force measurements, some pressure distribution measurements, and photographic observation. The experimental methods are described and the results given. Section III of this work gives a comprehensive account of the results and enables us to see how nearly the lift line and lift surface theories agree with the experimental results.

INTRODUCTION

The flow phenomena about plates and airfoils of short span are still not well known although such bodies are applied for airplane tail surfaces, ships' rudders, etc. In what follows will be given a description of a complete series of tests on such bodies, the results of which may be applied for all practical needs.

I. OBJECT OF INVESTIGATION

Though the flow phenomena about plates and profiles of large span have received a good deal of attention, those about small span plates and airfoils have not yet been satisfactorily investigated and most of the data we possess were obtained on apparatus that is already outdated. There is, nevertheless, a large field of application for bodies of large aspect ratio F/b^2, where F is

---

*"Strömungsvorgange an Platten und profilierten Körpern bei kleinen Spannweiten." VDI - Special Issue (Aviation), 1936. Extract from Thesis. Complete work obtainable at the Institut für Hydro- und Aerodynamik of the Technical High School, Danzig

the projected area and b the span of the body, as, for example, ship rudders and airplane tail surfaces where it is desirable to have as large a transverse force as possible with favorable drag relations. Furthermore, the phenomena of flow separation and pressure equalization at the sides which play so prominent a part in these short-span bodies are of general significance for numerous other flow problems.

Since a theoretical treatment of these flow phenomena still meets with insurmountable mathematical difficulties, it is the object of this paper to extend and complete the tests carried out so far, so as to obtain results that may be applied for all practical purposes.

The characteristics of the flow are largely determined by the angle of attack and the shape of the plate or airfoil. As far as shape is concerned, there are essentially three determining factors: form of outline, profile section, and amount of warping. To determine the effect of these on the forces and flow pattern, is one of the main objects of this work which, however, will be confined to unwarped bodies. The tests were carried out under the stimulus and leadership of G. Flügel, at the wind tunnel of the Technical High School at Danzig. In addition to our own measurements and observations, there were also evaluated the test data obtained by other coworkers in the same field at the Flow Institute. A short report on some of this work will be found in reference 1.

II. TESTS

1. Shapes and dimensions of investigated models.- The models investigated fall into two groups: thin flat plates and cambered, mostly symmetrical models. Their determining characteristics are given in tables I and II. (See p. 31, 32) The tunnel velocity was always in the direction of the plane of symmetry.

The following plan forms were used for the flat plates: rectangular, elliptical, semielliptical, and triangular (the last two were used for two different wind directions). The plates were entirely of 3.5 mm (0.138 in.) sheet brass, the upper surface being well ground. To reduce as far as possible the effect of finite thickness at least for the larger angles of attack, the plates were made sharp at one edge on the suction side (fig. 2).

The effect of the symmetrical camber was investigated only for the rectangular shape, the profile form being kept the same while the aspect ratio was uniformly increased. For the aspect ratio $F/b^2 = 1/1.0$ a thicker profile was obtained by increasing the height of the Gottingen profile 409. The thickness at all points was increased proportionately, so that for this case as well as for $F/b^2 = 1/1.14$, the effect of the thickness ratio could be made out at least on two unequal Joukowski profiles.* All models of this first set had flat side edges.

In another set of tests the same models (except the Joukowski profiles) were measured with rounded side edges. With models R.P.1a, R.P.2a, R.P.5a, and R.P.7a the rounding began at a distance from the side edge equal to 80 percent of the largest profile thickness, with R.P.6a at 100 percent. Figure 1 shows the amount of rounding which turned out to be most effective for model R.P.5a. Nonsymmetrical camber was investigated only for a circular outline (model E.P.1).

2. Method of conducting test.- With few exceptions the tunnel tests were made at a jet velocity of about 28 meters per second (63.2 miles per hour). The Reynolds Numbers (referred to the maximum chords of the models) were between the values $Re = 0.3 \times 10^6$ and $Re = 1.7 \times 10^6$. As several control tests showed, the forces and therefore the flow pattern about flat plates are practically independent of the Reynolds Number even for small values, thus making possible the application of the test results to larger models. Cambered models, however, may show the effects of the characteristics.

The pressure measurements at the plate surface were taken with a sounding device that consisted essentially of a small brass tube of 1.0 mm (0.04 in.) outer diameter which transmitted the static pressure to a Fuesz alcohol manometer. The forward end of the tube was closed by a semicircular stopper, and at 3.5 mm from the end of the tube was provided with a 0.4 mm (0.16 in.) boring for taking up the pressure. It is necessary to set the apparatus as far as possible parallel to the streamline direction. At larger angles of attack it is rather difficult, on account of the strong turbulence, to set the plate edges parallel to the average stream direction.

*Joukowski profiles are obtained, as is well known, by conformal transformations.

The flow-picture studies were made partly by means of observations on streamers. On the suction side this method is applicable only at small angles of attack; at larger angles the threads roll up on account of the strong eddies. In this case smoke tests were found to be of advantage. For producing the smoke, ammonia and concentrated hydrochloric acid in combination with compressed air were used.

To render the flow at the boundary layer visible, the method of Fales (reference 2) was applied to advantage. The upper surface of the plate was spread over with a mixture of soot and petroleum. When the flow is set up the petroleum evaporates and the soot follows the stream lines. This method was found to be very useful and failed only where the flow velocity was very small.

3. Force measurements.- The polars, moment coefficients, and normal force coefficients (the latter only for rectangular plates) are arranged in groups for each shape. In computing the air-force coefficients and the angles of attack, the effect of finite jet diameter was corrected for using the method of Prandtl-Glauert (reference 3). The corrections were for the most part below 1 percent. The moment coefficients were referred to the maximum chord of the model.

A. Flat Plates:

a) Rectangular plates (figs. 2, 3, and 4) (reference 4). The polars (fig. 2) show for equal values of lift coefficient c_a, an increase in the drag coefficient c_w with decreasing span, as may be expected from the airfoil theory of Prandtl. Correspondingly, in figure 3, at equal angle of attack α, there is a decrease in the normal-force coefficient c_n with increasing aspect ratio F/b^2.

Within the range of small angles of attack α. the increase in lift with span for $\alpha = 0$ is to be ascribed to the beveled edge on the suction side, which acts as an unsymmetrical camber on the plate. If we consider, to a first approximation, the plate to be replaced by its center line, we have a sharp-edge broken profile whose camber ratio for equal area, plate thickness, and beveling increases with increasing span. In the ideal case of infinitely thin, flat plates for any shape of outline, the c_n curves (fig. 3) all start at the origin and with increas-

ing angle of attack, gradually go over into the measured curves; the profile effect of the beveling is only evident at relatively small angles of attack.

A characteristic feature of the curves of normal-force coefficient is that for small values of F/b^2 they approach linearity and with increasing values curve more and more. This fact indicates a transition range of the flow which at one end of the range approaches the simple two-dimensional flow $(F/b^2) = 0$ and at the other end approaches a limit at which, with $F/b^2 = \infty$, the forces evidently follow the $\sin^2$ variation (reference 5) with angle of attack.

A peculiar behavior is shown at the plate with $F/b^2 = 1/0.66$ in the range of angle of attack between 45^0 and 49^0. In this case we find an isolated branch of the polar curve leading to very large air forces and lying in the projection of the normal polar curve. The tangential force coefficients, depending not only on the viscosity coefficient but also on the very small difference in pressure between the front and rear edges, were not computed. Their absolute values are small compared to the normal coefficients, except near $\alpha = 0$, so that the force was practically normal to the plane of the plate.

b) Elliptic plates (figs 5 and 6).- In the lower range up to a lift coefficient of about 0.9 the polar as well as the normal-force curves are very similar to the corresponding curves for the rectangular plate. If the lift-line theory is still assumed to hold true also for these spans and for small angles of attack, then theoretically the drag coefficient for the elliptic plate, for example, at $F/b^2 = 1/2.0$ would be, at the most, about 2 percent smaller than for the rectangular plate. The beveling on the suction side makes the plate have a larger camber ratio at the rim. This further causes the lift distributions for elliptic and rectangular plan forms to approach each other. The polars, too, show almost complete agreement in the lower range.

While there was a steady increase in the maximum lift with decreasing span up to $F/b^2 = 1/0.66$ for the rectangular shape, there was a marked unsteadiness in the case of the elliptic form. At $F/b^2 = 1/2.0$ and $F/b^2 = 1/1.8$, the maximum-lift coefficient is about 0.95 and suddenly increases at $F/b^2 = 1/1.62$ to 1.42. The models with $F/b^2 = 1/1.27$ (circular plate), 1/1.0, and 1/0.81 ap-

proach, above the angle of attack of 20°, a mean polar and normal-force curve which almost agrees with the curve for the square plate. At $F/b^2 = 1/0.81$ there is a similar unsteadiness, as in the case of the rectangular plate with $F/b^2 = 1/0.66$.

c) Semielliptic and triangular plates (figs 7 to 13).- For equal span more favorable results are almost always obtained with the straight edge used as trailing edge. Not only is the drag lower at equal lift but in most cases there is also a larger maximum value for the lift. It appears moreover that with the ellipse or broken edge of the triangle used as leading edges, the same forces are obtained at smaller angles of attack than with the straight sides as leading edges.

On a physical basis the reason for these deviations in the aerodynamic effect may be explained as follows: If both of these forms are replaced by their lift lines (that is, the lines joining the centers of pressure of the profile sections), which should be assumed at about t/4 from the leading edge, the curves of figure 11 are obtained. It then appears that the more important middle portion of lift line 2 is more removed from the effect of the trailing vortex sheet, so that in this case there arise smaller downward velocities. Form 2 therefore in comparison with 1, leads to greater effective angles of attack at equal geometric angle of attack and hence the agreement with the observed effect.

B. Cambered Models (figs. 14 to 20).

Symmetric models with Göttingen profile 409 (thickness ratio 12.6 percent) and with rectangular plan form were tested, using aspect ratios $F/b^2 = 1/2.0$, $1/1.5$, $1/1.0$, and $1/0.5$ (figs. 14 to 17). The side edges of the model were first provided with a plane bounding surface parallel to the mid plane. In the lower region up to a lift coefficient of about 0.50, the polars were similar to those of the flat plates. For equal aspect ratio the polars in each case almost coincide. In the upper range the cambered airfoils showed themselves to be considerably less favorable. Between $\alpha = 14.5°$ and $22.5°$, depending on the aspect ratio, there is a critical angle above which all polars show a strong increase in drag. At $F/b^2 = 1/2.0$ and $1/1.5$ flow separation sets in, whereas at $F/b^2 = 1/1.0$ and $1/0.5$ the flow essentially adheres to the model in spite of increased separation. The maximum lift for all airfoils was

considerably less than that for the plates. Using other thickness ratios and profile sections, rectangular shapes were investigated at $F/b^2 = 1/1.14$ (fig. 18), and $F/b^2 = 1/1.0$ (fig. 19). With $F/b^2 = 1/1.14$, the Göttingen profiles 429 (d/t = 11.5 percent) and 539 (d/t = 22 percent) were used. With $F/b^2 = 1/1.0$, Göttingen profile 409 was modified to give a thick profile (d/t = 19.4 percent). For each aspect ratio the greater thickness ratio gave the higher maximum lift, a result which was also obtained in the same range of thickness ratio with large spans (reference 6). The limited number of tests does not, naturally, permit any conclusions as to the effect of a variation in profile section. The fact that the shape of profile does play an important part is shown by the break in the polars of profiles 409, which is very marked at $F/b^2 = 1/1.0$ and 1/0.5 (figs. 16 and 17), but which at about equal thickness ratio does not appear with Göttingen profile 429 (fig. 18), and therefore must be considered as due to the form of profile.

A change in the form of the side edges appeared to be of significance only where there was a strongly developed flow at the sides. Thus, tests showed that with $F/b^2 = 1/2.0$ and 1/1.5, any rounding of the edges was almost without any effect. The effect was greater for $F/b^2 = 1/1.0$ and 1/0.5, but it showed up strongest in the case of the square airfoil having d/t = 12.8 percent (fig. 16), in which case there was a considerable increase in lift. For the other models (figs. 17 and 19), rounding of the side edges had the reverse effect. The fact that the characteristic discontinuity of the polars was independent of the shape of the side edges, shows that it is determined chiefly by the phenomena at the middle of the plates; that is, by the separation at the profile.

Of the unsymmetric profiles, only the circular cap having d/t = 10 percent was investigated (fig. 20). Compared with the circular plate, the polars show considerable improvement.*

4. Pressure measurements.- A deeper insight into the manner of force distribution is indispensable for the solution of many problems, especially those concerned with

*Compare with results on model with semielliptical outline and sickle-shaped profile in reference 1, figure 6, p. 320.

strength computations. It is important, too, to know the distribution of the "pressure hills" and "pressure valleys" on the suction side, since it gives us information on the flow pattern. The position and magnitude of the negative pressure maxima are important in connection with the danger of cavitation, for example, in the case of water propellers; and moreover when it is desired to know whether the flow at these positions has attained or exceeded the velocity of sound, which fact would make special precaution measures necessary to avoid harmful phenomena that would accompany this flow.

Since the lower side of the plate is always a stream surface, the pressure distribution at all sections is a simple continuous curve, and the flow phenomena should be essentially easy to understand. The suction side, on the contrary, is predominatingly covered with vortex layers and is therefore subject to nonuniform and time-varying pressure distribution, and these phenomena play the more important part. In the literature on the subject only the tests made some time ago by Gramont (reference 7) could be found and his results depart considerably from those obtained more recently. Evidently there were large sources of error arising from the set-up of his apparatus. The pressure measurements discussed below were taken recently at the Flow Institute of the Technical High School at Danzig.

Pressure-distribution measurements were taken on the suction side of the rectangular model using $F/b^2 = 1/1.0$ and $1/0.134$ for the angles of attack of 8° and 30°.* In general, for all plates there appeared at the beveled edges on the suction side sharp points of negative pressure which were particularly evident at small angles of attack with smooth flow, and which had considerable effect on the aerodynamic forces. At large angles of attack, however, the edges lie for the most part within the region of separation and therefore have slight effect.

A. Flat Rectangular Plate with $F/b^2 = 1/1.0$ (figs. 21 to 23).

For $\alpha = 8^\circ$ (fig. 21), the pressure distribution is constant all along the span except at the side edges where it is disturbed. Here there is a great increase in the negative pressure which is evidently due to the side flow at the plate. Except for the disturbances at the forward edge due to the beveling, there is an almost uniform de-

*Measured by J. Schmedemann.

crease in the negative pressure from forward to rear edge. The smallest negative pressure is at the middle of the plate at a distance $t/4$ from the trailing edge.

In figure 23 is shown the normal-force distribution obtained from the tests along the half span compared with the theoretical lift line. It was allowable in the theoretical results, since the angles of attack were small, to set the normal-force coefficient equal to the lift coefficient. The general character of the experimental lift distribution over the span on the pressure side was obtained from the work of Gramont (reference 7), which may be assumed to give approximately correct values within the region of small angles of attack. The theoretical lift distribution was determined by Glauert's method (reference 3). Under the effect of separation entirely different relations were obtained at an angle of attack of 30° (fig. 22). The points joining the relative negative pressure maxima arrange themselves to form a horseshoe-shaped hill on the plate and near the rear edge, include a region of pressure rise. The strongest negative pressure is found at a distance about $t/4$ from the forward and side edges. Figure 23 also shows the normal-force distribution on the suction side for $\alpha = 30^\circ$.

B. Flat Triangular Plate with $F/b^2 = 1/4.0$.

Pressure-distribution measurements were taken for each direction of flow. In general, these tests made it evident that at those positions of the plate where side flow may be expected, that is, at the discontinuous forward edge and the discontinuous rear edge, there is a decrease in pressure at the bottom side and an increase in negative pressure at the top. Figure 24 shows the lift distribution for the half span.

5. Investigations by means of flow pictures.- It should be remarked that the interpretation of the pictures of the boundary-layer flow should be taken with caution since the fluid in the boundary layer in regions of strong pressure variations possesses a type of motion very different from the motion in the neighboring fluid. See, for example, reference 8. Usually it took about three minutes for the coloring to spread out along the stream lines over the whole plate.

Since our space is limited, only a small part of the results obtained will be given. At very small angles of

attack the vortex layer on the suction side is still not very thin. There is, indeed, an equalization of pressure over the side edges but producing only insignificant separation, so that there is practically adhering flow. On the pressure side there takes place, on account of the pressure drop at the side edges, an outwardly directed cross velocity which increases with increasing angle of attack and aspect ratio (fig. 25). The manner of distribution over the plate depends essentially on the plan form. In general, there is observed an increasing cross flow as the side and front edges are approached. The fluid at the side edges flows spirally, forming a "vortex braid" whose position, magnitude, and extent are determined by the plan form, aspect ratio, and angle of attack.

We shall first discuss the flow phenomena at the suction side of the rectangular shape. The character of the flow is also the same for all other plan forms. As a result of the separation, there is formed at the middle of the plate a "vortex cushion" whose dimensions depend essentially on the angle of attack and the aspect ratio. In figures 26 and 27 this is shown for $F/b^2 = 1/1.0$ and $1/0.5$ at the same angle of attack of 18°, and in figure 28, a boundary-layer photograph at the mid plane of the plate with $F/b^2 = 1/1.0$ and 30°. At small aspect ratios within the range of nonseparation this vortex cushion can spread out along the whole chord length, whereas for large aspect ratios, it remains confined to the forward part of the plate.

So long as there is no separation of flow, the end vortices travel nearly parallel to the plane of the plate downstream (fig. 29). Only at large aspect ratios do they form a small angle with the plate since the fluid behind the plate rolls up about the core and therefore the core is gradually forced away from the plate. At very small spans as, for example, where $F/b^2 = 1/0.033$, the after part of the curled trailing vortex becomes unstable (at $F/b^2 = 1/0.033$ from about 10° on). At larger angles of attack, there is a definite break approximately in the direction of the blower velocity. With increasing angle of attack this break travels forward and at 16°, for example, (fig. 30), it is at about 40 percent of the chord from the end of the plate. Behind this position there is separation without spiral formation.

The phenomena at the boundary layer itself may be seen from figures 31 and 32 for $F/b^2 = 1/1.0$ and $1/0.5$. It may

be seen that a sickle-shaped region of stagnation separates the vortices at the forward region of the plate from those behind and at the sides. In the forward portion there is back flow and further up at the front edge there is cross flow which at the side edges bends into the stream direction. Evidently, at this position the vortex cushion is broken up by the rolled-up vortices. The cross flow of the stream lines at the side edge similarly shows that considerable quantities of fluid from the suction side are rolled up into the "vortex braids" and in this way the vortex cushion at the rear of the plate is carried away. After separation of the flow there is a considerable increase in the space occupied by the vortices (fig. 33).

The flow field for the elliptic form shows great similarity with that of the rectangular form and is but slightly changed by the different outline. Whereas, in the case of the rectangular plate, the vortex braids arise at the two forward edges - in the case of the elliptic plate they arise at a certain distance behind the forward edge, which distance grows less with increasing angle of attack. The vortex braids must naturally follow the side edges and are therefore curved. The vortex cushion, especially at large values of F/b^2, narrows down at the front on account of the decreasing width of the plate. The entirely different nature of the side vortices for the semielliptic and triangular plan forms, which arises from the change in the direction of flow, is clearly seen in the boundary-layer photograph.

III. RESULTS AND CONCLUSIONS

1. Rectangular plates.- For flat plates of given shape, the flow pattern is practically independent of the Reynolds Number except for small values (which, however, were not used in our work) but does depend to a large extent on the aspect ratio and the angle of attack.

In the following discussion we shall consider more closely the nature of the dependence on these two deciding factors. It is possible to divide up the angles of attack and aspect ratios into certain sets or ranges within which the flow pattern shows uniform characteristics. The following ranges may be distinguished:

Range 1: $F/b^2 < 1/2.0$

a) At small angles of attack there is the Prandtl type of flow.

b) At larger angles of attack up to 90° there is separated flow (at very small aspect ratios there is also the formation of a von Kármán vortex street).

Range 2: $F/b^2 = 1/2.0$ up to about $1/0.1$

a) Prandtl type of flow at very small angles of attack.

b) At larger angles up to separation there is strongly separated flow along the middle of the airfoil together with a strongly developed airfoil tip flow at the sides.

c) At very large angles of attack up to 90° detached flow without side vortices.

Range 3: F/b^2 = about $1/0.1$ up to infinity.

a) At very small angles of attack the usual airfoil type of flow.

b) At larger angles of attack normal airfoil-type flow at the forward part of the plate with separated flow along the after part (with the probable formation of a vortex street if the after part is sufficiently long). With increasing angle of attack the extent of the separation increases, spreading more and more until, after a certain angle of attack is exceeded, there is no more airfoil-type flow at the forward part.

c) Separated flow up to 90° (probably with the formation of a von Kármán vortex street, whose vortex filaments are parallel to the plate edges).

It should be remarked that sharp transitions occur only when there is separation; in all other cases there is almost always a gentle transition from one flow pattern to another, which is also the case when, for example, two

different types of flow are set up at the plate side by side at equal angle of attack.

The most important features of the flow within each range will now be discussed.

Range 1(a), ($F/b^2 < 1/2.0$).- The flow phenomena within this range, with the Prandtl type of flow at small angles of attack, are well known and the airfoil theory may, with a sufficient degree of accuracy, be applied to compute the aerodynamic forces.

Range 1(b), ($F/b^2 < 1/2.0$).- A well-defined separation of flow and no further increase in the normal force with increasing angle of attack clearly mark the limits between ranges 1(a) and 1(b). Within range 1(b) the large vortex field behind the plate is essentially parallel to the undisturbed flow direction. With sufficiently small values of F/b^2 and at large angles of attack, a von Kármán vortex street is set up. Figure 34 shows the variation of the normal lift coefficient for flat plates, the data being mostly those obtained at Göttingen.

Range 2(a), ($F/b^2 = 1/2.0$ up to about $1/0.1$).- At small angles of attack the flow may be considered to be of the Prandtl airfoil type of flow. On account of the increase in the flow at the edges with increasing aspect ratio, the angles of attack up to which the lifting line theory agrees with experiment decrease with increasing aspect ratio.

Range 2(b), ($F/b^2 = 1/2.0$ up to $1/0.1$).- Within this range the flow may be considered essentially as divided into two parts, namely, the "wing center flow," which is accompanied by separation and the "wing-tip flow." With small aspect ratios the former type of flow predominates; with increasing aspect ratio as well as angle of attack, this type recedes into the background and gives way to the "wing-tip flow" and is almost entirely replaced by the latter at the other limit of the range of F/b^2.

For equal angles of attack there is an increase in the diameter of the side trailing vortices with increasing aspect ratio, and these vortices are therefore more effective at the after part of the plate than at the forward part. The induced transverse flows at the after part on the suction side reduce the tendency toward separation. As a result of this induction, considerable masses of air

are involved in vortex motion along the side edges on the suction side (figs. 31 and 32), so that by the gradual elimination of the vortex masses downstream, the main flow again becomes adhering. These phenomena prevent to a considerable degree the complete separation of the flow; that is, make separation appear at a considerably larger angle of attack. Separation is not, however, avoided entirely, since vortices continue to break through downstream. At any rate, the place where the flow begins to adhere again can be clearly made out on the back side as a stagnation region from which the stream lines spread out in all directions (figs. 31 and 32). With increasing angle of attack this region moves farther downstream. At smaller values of aspect ratio, there occurs the case where after a certain angle of attack is exceeded the stagnation region would lie behind the plate and from here on there is naturally separated flow. This mode of separation is accompanied by a strong decrease in the normal force. At larger values of F/b^2 separation evidently sets in, starting from the side edges. In the case of the long plates, the diameter of the trailing vortices becomes so big that apparently no more fluid can be rolled up at the plate ends. There then follows at the after part of the plate a separation of flow which is limited in extent at first but with increasing angle of attack soon spreads over the whole plate. The process of separation sets in more gradually here than is the case with large values of F/b^2.

Under the effect of the wing-tip flow at equal angle of attack, there is a considerable change in the pressure distribution along the span and especially on the suction side. If there were no cross flow - that is, with $F/b^2 = 1/\infty$ - the pressure would be constant, line a, figure 35. With the usual flow about an airfoil of finite span, the theoretical pressure distribution, taking into account the induced cross velocity of the trailing vortex surface, is along the line b. As soon as strong cross flow is set up, which is the case for small spans, there takes place on the suction side, under the effect of the separation, a shifting of the pressure along line c. Within this range there is always a strongly modified pressure distribution, depending on the aspect ratio and angle of attack.

The center flow within this range is always accompanied by separation. The thickness of the vortex cushion on the suction side depends very much on the aspect ratio and the angle of attack. As long as there is not separa-

tion of the main stream, the vortex cushion has a definite camber effect; hence, the high lift coefficients.

Range 2(c), (F/b^2 = 1/2.0 to about 1/0.1).- The lower limit of this range, similar to case 1, is marked by a sharply defined separation. Measurements were made up to moderate angles of attack only. Since within this range of aspect ratios the normal lift coefficients for 90° show only small changes, no large variations in force should be expected at the large angles of attack. Deviations are found immediately after separation of flow sets in and these are explained by the local variations in the flow at the forward and side edges.

Range 3(a), (F/b^2 = about 1/0.1 to infinity).- At very small angles of attack there still takes place the usual airfoil flow. The edge vortices lie along the entire length. Only a small vortex cushion can be built up at the narrow leading edge. The upper limit of the range is given by that position at which the rolled-up vortices at the sides suddenly turn aside from the plate and bend approximately in the direction of the stream. The larger the F/b^2, the smaller the range of angle of attack over which this range extends.

Range 3(b), (F/b^2 = about 1/0.1 to infinity).- The distinctive feature of this range is the broken-edge vortex (fig. 30). The larger the angle of attack, the shorter the distance along which the rolled-up side vortices adhere to the plate. The reason for the breaking off of the side vortices is obviously the fact that the diameter has become too large compared to the width of the plate. Behind the position of the break a condition of flow is set up similar to the normal flow about a plate but with the difference that the flow takes place diagonally across the plate. If this after region is sufficiently long, there is probably formed a Kármán type of vortex street with vortex filaments parallel to the side plate edges. After a certain angle of attack is exceeded, there is no more rolled-up vortex formed at the forward part of the plate, which fact leads to a relative decrease in the pressure difference between the forward and after sides.

As may be seen from figure 34, for F/b^2 = 1/0.033, a weak form of separation may be made out (at $\alpha \approx 45°$). This point marks the limit of this region.

Range 3(c), ($F/b^2 = 1/0.1$ to infinity).- Here there is completely separated flow without rolled-up vortices. In the limiting case $F/b^2 = \infty$, the normal-force coefficient should depend on the angle of attack according to the $\sin^2$ law of Flügel (reference 9). For the plate $F/b^2 = 1/0.033$, this relation holds only approximately, since on account of the finite chord a flow takes place about the forward edge. In figure 34 are shown the results of the tests on the plate $F/b^2 = 1/0.033$ compared with the values obtained from the $\sin^2$ law. That the $\sin^2$ law is followed to some extent, is clearly evident. The forces of the inclined plate of infinite chord actually follow the $\sin^2$ law; at the same time there is set up a type of flow behind the plate which may be considered as a Kármán vortex street with diagonal vortex filaments.

2. Elliptic plates.- On account of the approximately similar character of the flow the same conclusions can be applied in this case as for the rectangular form. With equal aspect ratio and angle of attack, the forces on both forms are therefore similar.

At small angles of attack and large spans within the limited region of application of the airfoil theory, the elliptic form, for equal aspect ratio and lift, should theoretically have a somewhat smaller resistance than the rectangular form. With $F/b^2 < 1$ this difference should be very small, as was also confirmed by experiment.

The higher maximum lifts obtained throughout with the elliptic form are explained by the different flow pattern in each case. Within range 2(b) where the vortex layer, at the small aspect ratios, is built up on the suction side, the travel of the dead-air region behind the plate is slowed down on account of the greater chord at the middle of the plate, and so, due to the longer vortex cushion, the maximum lift is increased. At the larger aspect ratios, on the other hand, the improved travel of the vortex masses on the suction side due to the small distance between the tip vortices, brings about higher aerodynamic forces.

3. Semielliptic and triangular plates.- The flow pattern about semielliptic plates, which always leads to higher lift forces if the straight edge is made the trailing edge, was already discussed above. The correctness of the results is confirmed by the pressure-distribution

measurements on the related triangular form, whose pressure distribution along the span may be assumed very similar to that of the semiellipse.

As in the case of the rectangular form, the high lift coefficients may here also be explained by the effect of the tip vortices. For each direction of flow there was considerable difference in the form of the side vortices and the position where they were set up. In each case they followed the side edges; with straight edge as leading edge, they bent inward, and with straight edge as trailing edge they bent outward. The lack of uniformity in the lift coefficients is essentially explained by the different stability relations of the curved side vortices.

The different manner in which the edge vortices behave for each flow direction results in entirely different flow relations. With the straight edge as trailing edge the fluid on the suction side is continually rolled up by the growing edge vortices; with the straight edge as leading edge, on the other hand, the vortex layer on the suction side is carried down principally by the vortex core. Evidently, in the latter case there is a higher turbulence which leads to increased resistance.

4. Cambered models.- The effect of the camber is to introduce the following essential changes as compared with the plates:

With adhering center flow, a much increased dependence of the forces on the Reynolds Number may be expected for the larger spans.

The camber on the suction side brings about a smoother flow along the middle of the model and reduces the formation of vortices.

The distance between the suction side and the pressure side is increased by the thickness of the profile. This brings about a decrease in the tip flow.

Although a region of separation is formed at the rear edge as in the case of flat plates, the favorable effect of the camber compared with the flat plates is shown by the improved polar curves. The strong decrease in the maximum lift coefficient is evidently due to the effect of the edge vortex, which is disturbed in its motion by the thicker side edges.

From the limited number of tests conducted, it is clear that considerable variations in the polars may be obtained by varying the longitudinal profile as well as the transverse profile. Within the region $F/b^2 = 1/2.0$ up to 1/1.5, a change in the transverse profile will still have little effect but the effect will increase as the span decreases. For a high maximum-lift coefficient a sharp side edge is better than a rounded edge because it permits a better rolling up of the side vortices.

The same conclusion is also reached from the measurements on the spherical cap. As may be concluded from the strongly decreased profile drag as compared with the circular plate, the vortex layer on the suction side is evidently kept very small as a result of the camber and, on the other hand, the sharp-edged rim appears to offer good conditions for flow. This effect explains the large angle of separation which even exceeds that for a flat plate by a small value.

IV. COMPUTATION OF THE FORCES FOR RECTANGULAR PLATES AT VERY SMALL ANGLES OF ATTACK

Since for large aspect ratios and very small angles of attack the plate surface may be considered as a surface of flow on account of the small thickness of the vortex layer at the middle portion and the small tip flow at the sides, it may be assumed that the theory is applicable for this range. The lifting line and lifting surface theory will be applied to the rectangular plate. With the aid of a Fourier series, Glauert obtains the equation:

$$\frac{dc_a}{d\alpha} = \left(\frac{dc_a}{d\alpha}\right)_\infty \frac{\pi}{4} \frac{A_1}{\mu\alpha} \tag{1}$$

where

$$\frac{A_1}{\mu\alpha} = \frac{1}{N} \cdot (593.971\ \mu^3 + 280.407\ \mu^2 + 40.388\ \mu + 1.777) \tag{2}$$

and

$$N = 593.971\ \mu^4 + 784.743\ \mu^3 + 272.771\ \mu^2 + 34.561\ \mu + 1.414 \tag{3}$$

Furthermore,

$$\mu = \frac{1}{4}\left(\frac{dc_a}{d\alpha}\right)_\infty \frac{t}{b} \qquad (4)$$

$\frac{dc_a}{d\alpha}$ denotes the value of the slope for finite span of the plate, and $\left(\frac{dc_a}{d\alpha}\right)_\infty$ the value for infinite span. For a given value of $\left(\frac{dc_a}{d\alpha}\right)_\infty$, $\frac{dc_a}{d\alpha}$ is a function of t/b only. Figure 36 shows results computed from equation (1) compared with the test values. For values above $F/b^2 = 1/5.0$ the test points fall on the curve for $\frac{dc_a}{d\alpha} = 6.0$; for smaller values there is increasing deviation from the lift line theory. Similarly, the region of attack angles along which the c_a curves follow the tangent $dc_a/d\alpha$ narrows down with increasing F/b^2; with $F/b^2 = 1/2.0$, it includes 12° with 12 percent deviation and decreases almost linearly to about 4° at $F/b^2 = 1/0.5$.

The results from the lift surface theory, as computed by the Prandtl-Blenk (reference 10) method, are likewise shown in figure 36. At large aspect ratios the agreement is unusually good, but for small values of F/b^2, the theoretical results lie unexpectedly below the experimental values. To find an approximate relation that is valid over a larger range of angles of attack is outside the scope of this work.

Translation by S. Reiss,
National Advisory Committee
for Aeronautics.

REFERENCES

1. Kempf, G., and Forster, E.: Hydromechanische Probleme des Schiffsantriebs, p. 315. Springer, Berlin, 1932.

2. Wien, W., and Harms, F.: Handbuch der Experimental Physik, vol. 14, pt. I, p. 701. Leipzig, 1932.

3. Glauert, H.: Die Grundlagen der Tragflügel- und Luftschraubentheorie, p. 168. Springer, Berlin, 1929.

4. Foppl, O.: Jb. Motorluftsch.-Stud.-Ges., 1910-11.

5. Flachsbarth, O.: Ergebn. Aerodyn. Vers.-Anst. Göttingen, IV Lieferung, Munich and Berlin: Oldenbourg, 1932.

6. Flügel, G.: Über die Strömung an Platten und Plattenähnlichen Korpern. Schiffbau, vol. 30, 1929, p. 336.

7. National Advisory Committee for Aeronautics: Aerodynamic Characteristics of Airfoils - V. T.R. No. 286, N.A.C.A., 1928.

8. Gramont, A. de: Essai d'Aerodynamique du Plan. Librairie Hachette & Co., Paris, 1911.

9. Kopp, B. A.: Ermittlung räumlicher Strömungsvorgange mit Hilfe des Farbanstrichverfahrens. Diss. Techn. Hochsch., Hannover, 1933.

10. Flügel, G.: Schiffbau, vol. 30, 1929, p. 336.

11. Blenk, H.: Der Eindecker als tragende Werbelflache. Z.f.a.M.M., vol. V, 1925, p. 36.

TABLE I. Characteristics of Thin, Flat Plates

Model	Plan form	Aspect ratio F/b^2	Area cm^2
R.1	Rectangular	1/2.0	500.5
R.2		1/1.5	498.2
R.3		1/1.25	502.3
R.4		1/1.0	501.8
R.5		1/0.66	498.2
R.6		1/0.5	500.5
R.7		1/0.35	502.0
R.8		1/0.134	506.6
R.9		1/0.033	271.5
E.1	Elliptic	1/2.0	502.7
E.2		1/1.8	500.5
E.3		1/1.62	501.4
E.4		1/1.27	615.7
E.5		1/1.0	501.4
E.6		1/0.81	502.7
E.7		1/0.5	501.0
H.E.1	Semielliptic	1/2.55	488.0
H.E.2		1/2.0	500.7
H.E.3[1]		1/1.75	498.0
H.E.4		1/1.45	516.0
H.E.5		1/1.0	506.1
H.E.6[1]		1/0.66	500.0
D.1[2]	Triangular	1/4.0	501.7
D.2		1/2.31	506.4

1) Measurements made by J. Schmedemann.

2) Measurements made by A. W. Quick.

TABLE II. Characteristics of Cambered Models

Model	Plan form	Aspect ratio F/b^2	Thickness d mm	Area cm^2	Thickness / chord %	Profile[1]
R.P.1	Rectangular with flat side edges	1/2.0	20	497	12.7	Gött.409
R.P.2		1/1.5	22.7	496.9	12.5	Gött.409
R.P.3		1/1.14	40.2	1402.9	11.5	Gött.429
R.P.4		1/1.14	77	1397	22.0	Gött.539
R.P.5		1/1.0	28.7	502.5	12.8	Gött.409
R.P.6		1/1.0	43.5	502	19.4	Gött.409 Modified
R.P.7		1/0.5	40	502.4	12.7	Gött.409
R.P.1a	Rectangular with rounded side edges	1/2.0	20	498.7	12.7	Gött.409
R.P.2a		1/1.5	22.7	497.2	12.5	Gött.409
R.P.5a		1/1.0	28.7	503.1	12.8	Gött.409
R.P.6a		1/1.0	43.5	502	19.4	Gött.409 Modified
R.P.7a		1/0.5	40	500.1	12.7	Gött.409
E.P.1	Circular	1/1.27	28	616	10	Suction side, circular arc; Pressure side. flat

[1] Ergebn. Aerodyn. Vers.-Anst. Göttingen, Lief. I to IV.

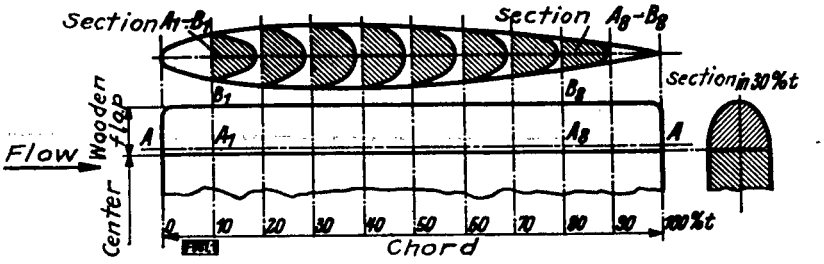

Figure 1.- Side rounding on model R.P. 5a.

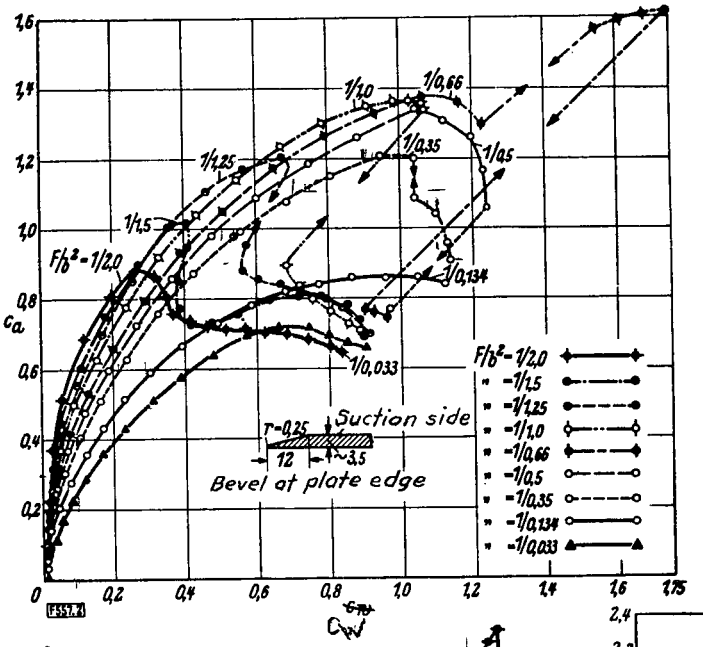

Figure 2.- Polars of plates with rectangular outline.

Figure 3.- Normal lift coefficients C_n of plates with rectangular outline.

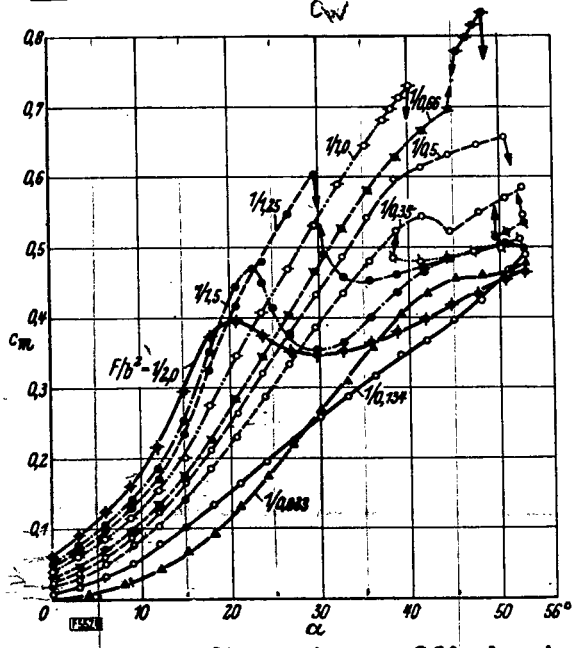

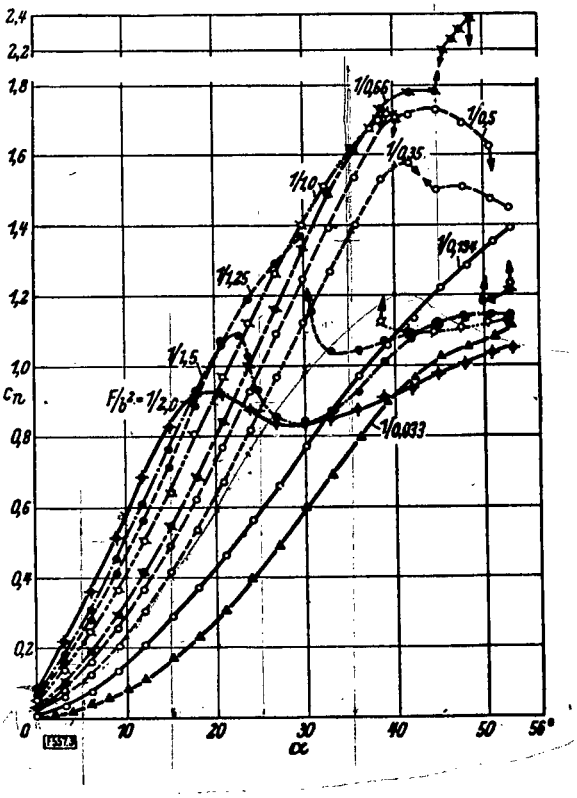

Figure 4.- Moment coefficients C_m of plates with rectangular outline.

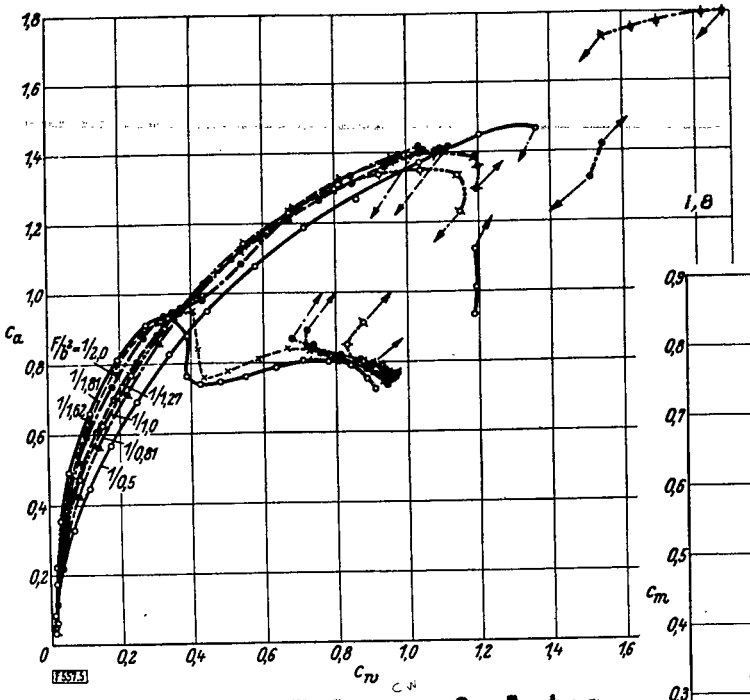

Figure 5.- Polars of plates with elliptic outline.

Figure 6.- Moment coefficients of plates with elliptic outline.

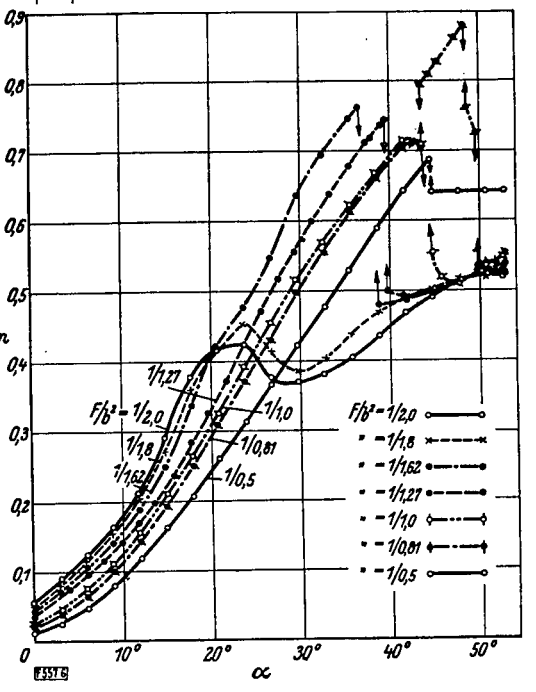

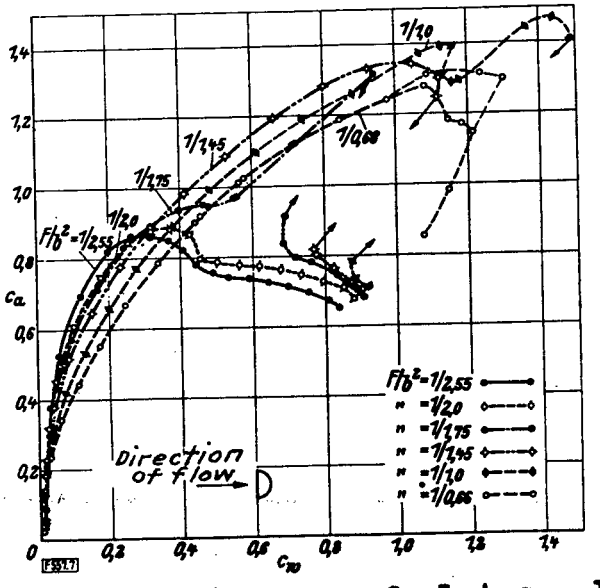

Figure 7.- Polars of plates with semi-elliptic outline and straight leading edge.

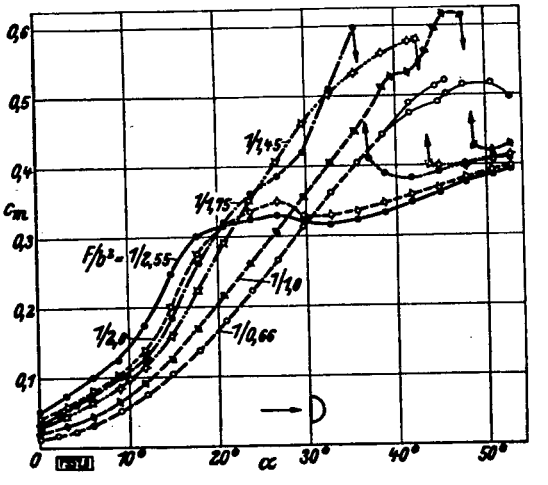

Figure 8.- Moment coefficients of plates with semi-elliptic outline and straight leading edge.

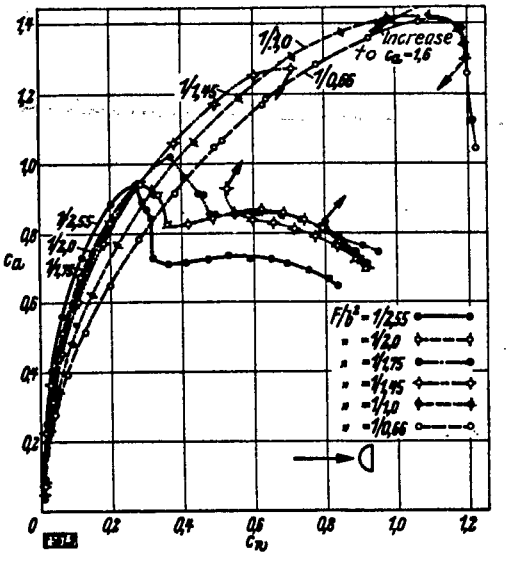

Figure 9.- Polars of plates with semi-elliptic outline and straight trailing edge.

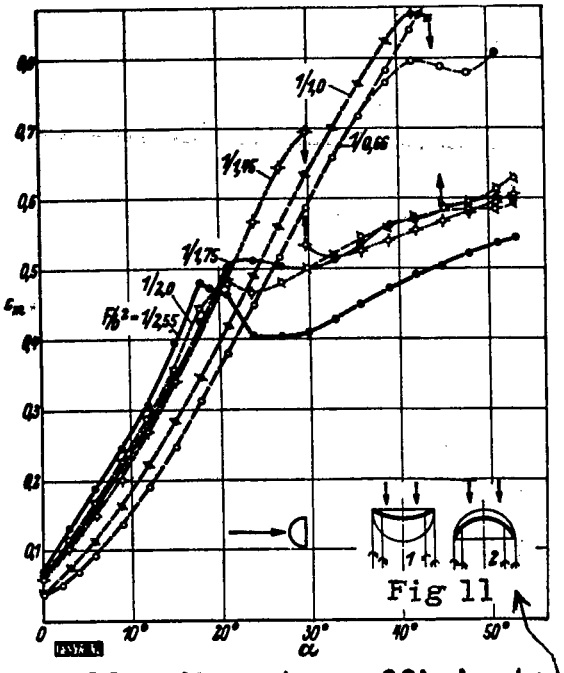

Figure 10.- Moment coefficients of plates with semi-elliptic outline and straight trailing edge.

Figure 11.- Forms of lift lines.

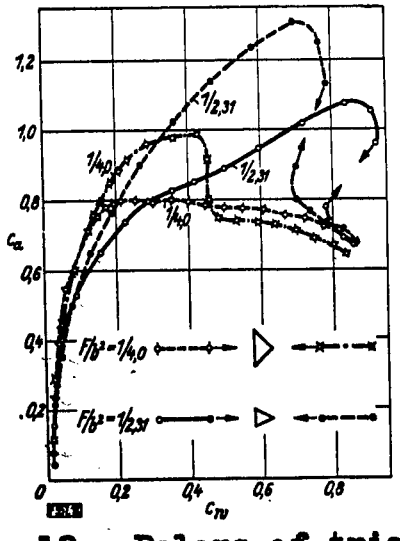

Figure 12.- Polars of triangular plates.

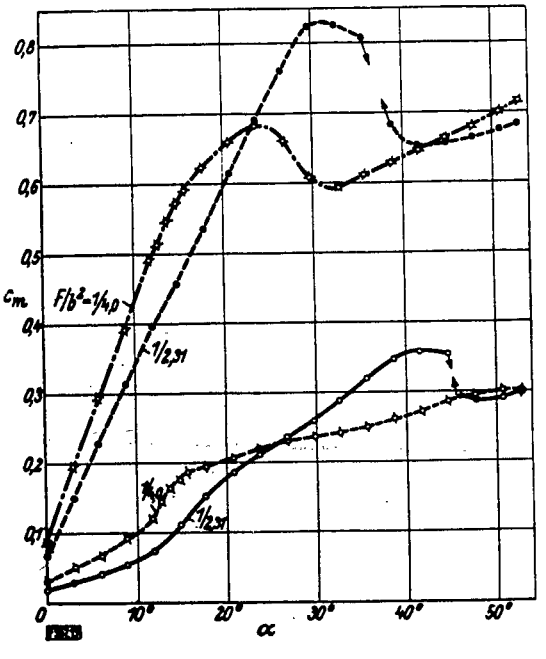

Figure 13.- Moment coefficients of triangular plates.

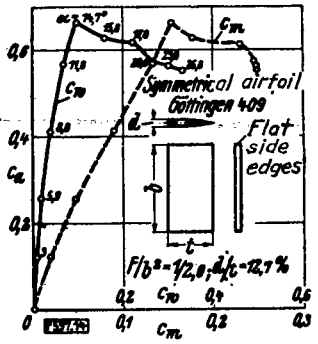

Figure 14.- Rectangular outline, $F/b^2 = 1/2.0$.

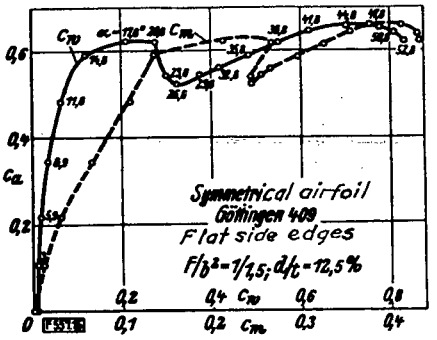

Figure 15.- Rectangular outline, $F/b^2 = 1/1.5$.

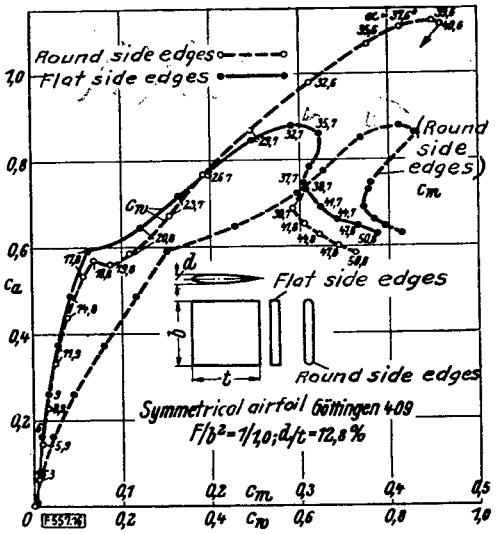

Figure 16.- Square outline $F/b^2 = 1/1.0$.

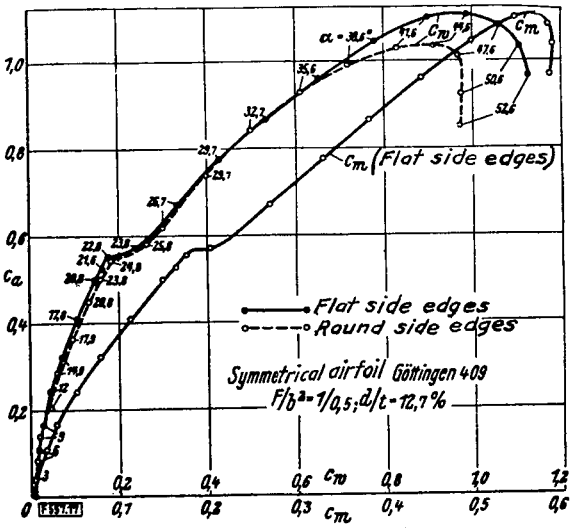

Figure 17.- Rectangular outline $F/b^2 = 1/0.5$.

Figures 14 to 17.- Polars and moment coefficients of cambered models, Göttingen profile 409.

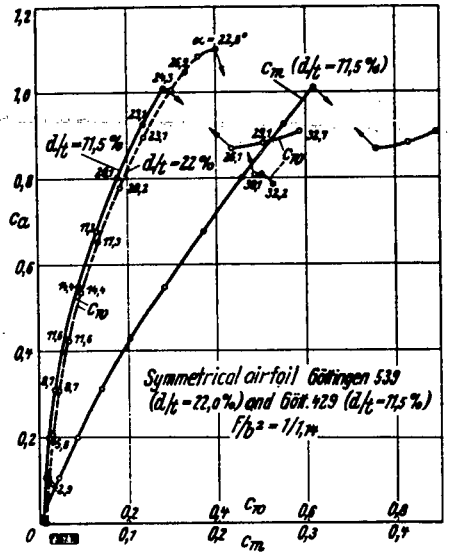

Figure 18.- Polars and moment coefficients of cambered models with rectangular outline, F/b^2 = 1/1.14 Göttingen profiles 539 and 429.

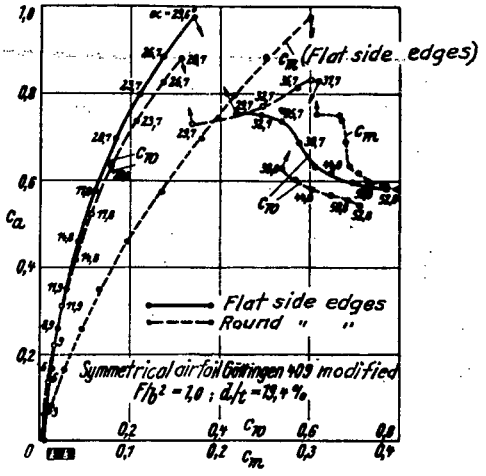

Figure 19.- Polars and moment coefficients of cambered models with square outline, F/b^2 = 1/1.0, Göttingen profile 409 made thicker proportionately.

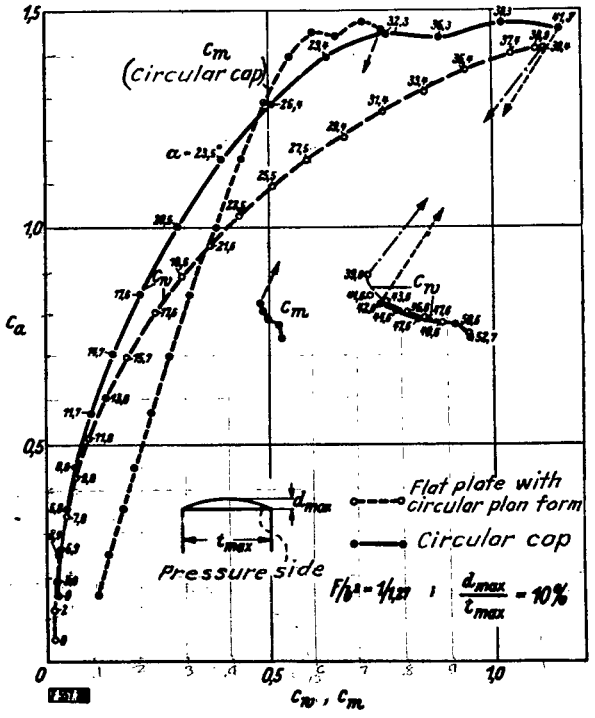

Figure 20.- Polars of spherical cap and circular plate and moment coefficients of spherical cap.

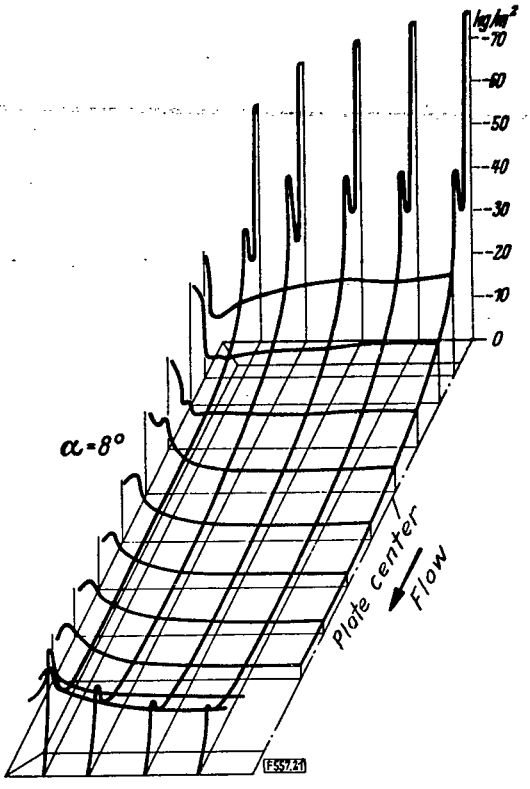

Figure 21.- Pressure distribution on the suction side of the square plate at 8° angle of attack.

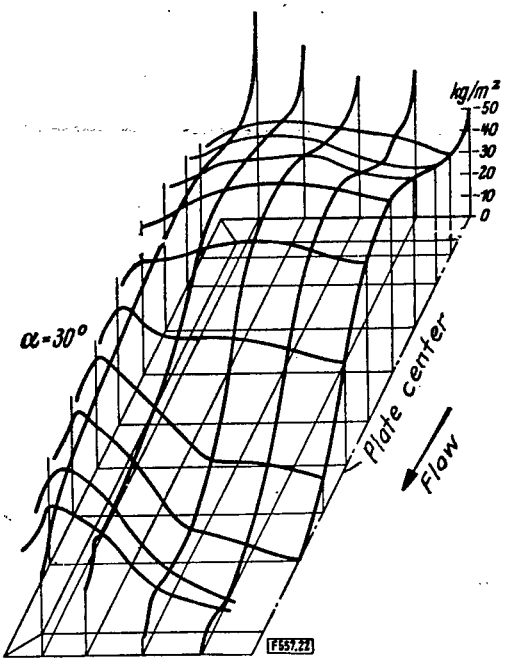

Figure 22.- Pressure distribution on the suction side of the square plate at 30° angle of attack.

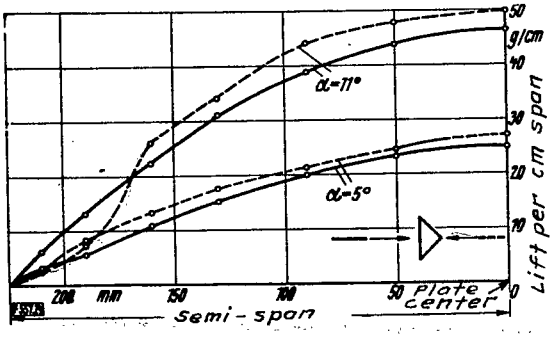

Figure 24.- Measured lift distribution over the span of a triangular plate, $F/b^2 = 1/4.0$.

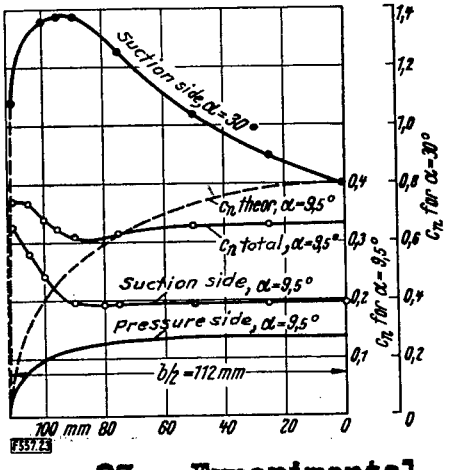

Figure 23.- Experimental and theoretical normal-force distribution over the span of a flat square plate.

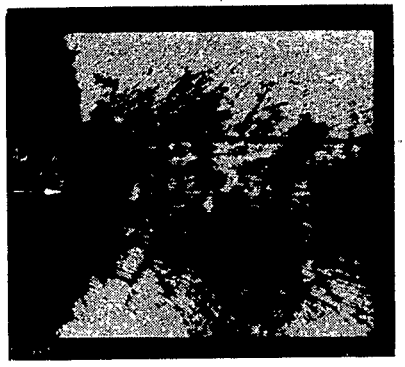

Figure 25.- Boundary-layer photograph of the pressure side of a flat plate, $F/b^2 = 1/1.0$; $\alpha = 38°$.

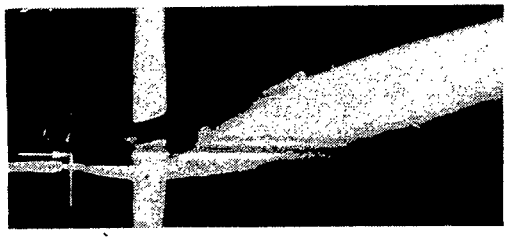

Figure 26.- Smoke picture of the flow at the center of a rectangular plate, $F/b^2 = 1/0.0$; $\alpha = 18°$.

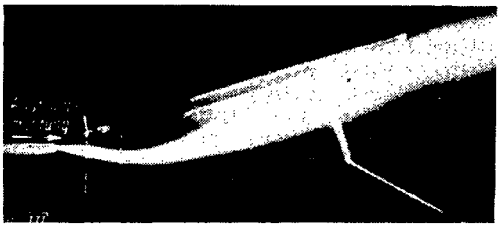

Figure 27.- Smoke picture of the flow at the center of a rectangular plate, $F/b^2 = 1/0.5$; $\alpha = 18°$.

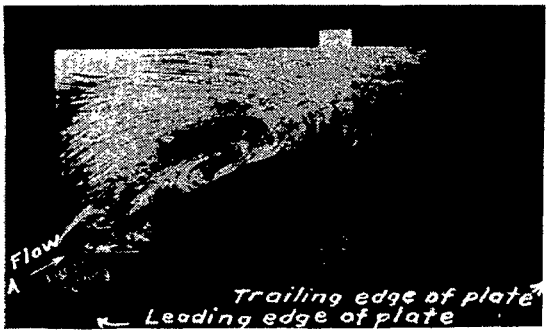

Figure 28.- Boundary-layer photograph of the flow at the suction side of a flat rectangular plate, $F/b^2 = 1/1.0$; $\alpha = 30°$.

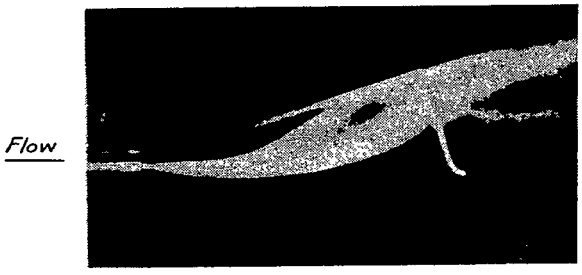

Figure 29.- Rolled up vortex at the side edge of a flat rectangular plate, $F/b^2 = 1/1.0$; $\alpha = 18°$.

Figure 30.- Vortex core at the side edge of a flat rectangular plate, $F/b^2 = 1/0.033$; $\alpha = 16^\circ$.

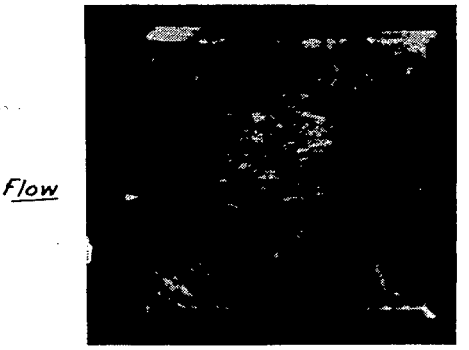

Figure 31.- Boundary-layer photograph of the suction side of a flat rectangular plate, $F/b^2 = 1/1.0$; $\alpha = 27^\circ$.

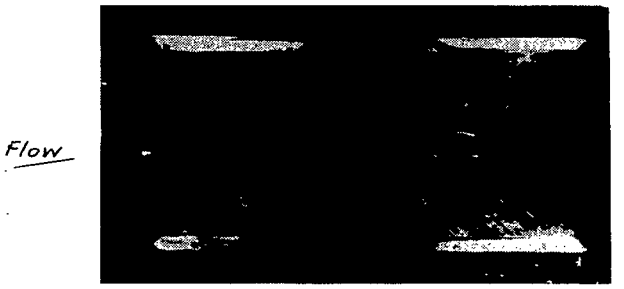

Figure 32.- Boundary-layer photograph of the suction side of a flat rectangular plate, $F/b^2 = 1/0.5$; $\alpha = 27^\circ$.

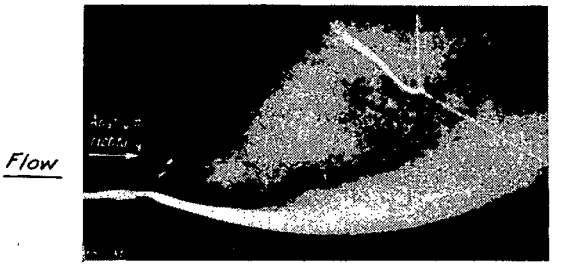

Figure 33.- Smoke picture of the suction side of a flat rectangular plate, $F/b^2 = 1/1.0$; $\alpha = 45^\circ$. Separated flow.

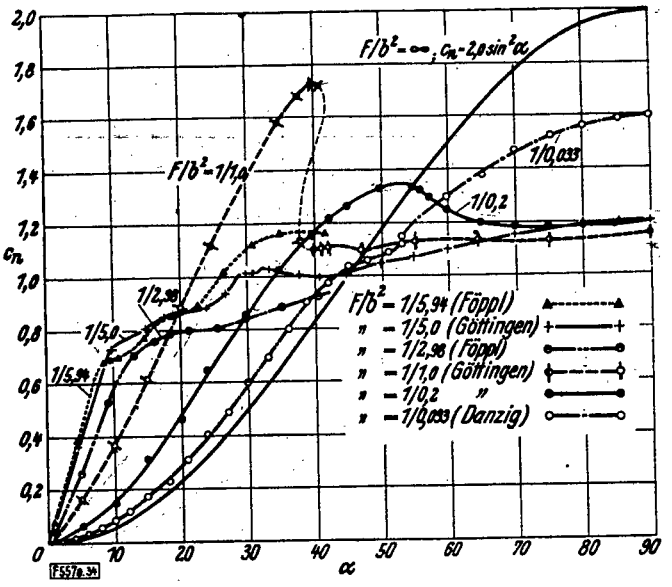

Figure 34.- Normal-force coefficients C_n for flat rectangular plates.

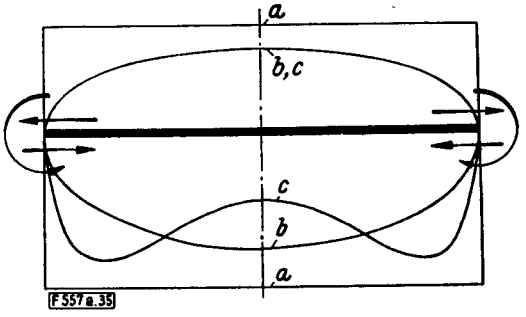

Figure 35.- Lift distribution over the span (schematic):
(a) $F/b^2 = 0$
(b) $F/b^2 = 2.0$
(c) $F/b^2 = 2.0$

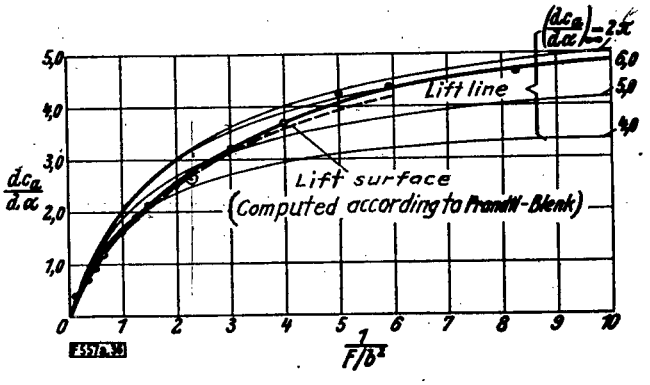

Figure 36.- Theoretical and experimental slopes $dC_a/d\alpha = f\ (F/b^2)$ for rectangular plates.